

# Generation of continuous-variable spatial cluster entangled states in optical mode comb

RONGGUO YANG,<sup>1,2,\*</sup> JINGJING WANG,<sup>1,2</sup> JING ZHANG,<sup>1,2</sup> KUI LIU,<sup>1,3</sup> AND JIANGRUI GAO<sup>1,2,3</sup>

<sup>1</sup>State Key Laboratory of Quantum Optics and Quantum Optics Devices, Shanxi University, Taiyuan 030006, China

<sup>2</sup>College of Physics and Electronic Engineering, Shanxi University, Taiyuan 030006, China

<sup>3</sup>Institute of Opto-Electronics, Shanxi University, Taiyuan 030006, China

\*Corresponding author: yrg@sxu.edu.cn

Received 4 August 2016; revised 23 September 2016; accepted 10 October 2016; posted 11 October 2016 (Doc. ID 273143); published 4 November 2016

Cluster entangled states are often used as the fundamental resources for one-way quantum computation. In this paper, we put forward a scheme of generating the spatial cluster entangled states of Laguerre–Gaussian modes in a large-Fresnel-number degenerate optical parametric oscillator operating below threshold with type I phase matching, which is pumped by two spatial Laguerre–Gaussian modes with the same frequency. The nonlinear parametric process of each pump mode satisfies momentum, energy, and orbit angular momentum conservation. Eleven-partite spatial cluster entangled states of Laguerre–Gaussian modes can be produced in the optical mode comb under feasible experimental condition, which can be demonstrated by using the entanglement criterion proposed by van Loock and Furusawa. © 2016 Optical Society of America

**OCIS codes:** (190.4410) Nonlinear optics, parametric processes; (270.2500) Fluctuations, relaxations, and noise; (270.0270) Quantum optics.

<http://dx.doi.org/10.1364/JOSAB.33.002424>

## 1. INTRODUCTION

Quantum entanglement has been extensively applied in quantum information fields, such as quantum teleportation, quantum dense coding, and quantum key distribution [1–3], etc. Multipartite entanglement poses a fundamental challenge in the quantum system, because it is ubiquitous to any of the quantum computation algorithms and quantum communication protocols [4]. There are two typical continuous-variable (CV) multipartite entanglement states: cluster entangled states [5,6] and Greenberger–Horne–Zeilinger (GHZ) entangled states [7,8]. Cluster entangled states are special entangled states and have large entanglement persistency (in the case of  $N > 4$ ), which are more difficult to be destroyed by local operations than GHZ states [9]. As an important resource in many branches of physics, cluster entangled states not only can be used as a medium to transfer quantum information in quantum communication protocols, but also can speed up computation in quantum algorithms. Therefore, the research on the generation of cluster entangled states has become one of the most crucial works nowadays.

In order to realize measurement-based quantum computation, quantum information processing and spatial quantum image, large-scale CV cluster entangled states have aroused much interest in theory and experiment. Quantum optical frequency comb is one of the most effective ways to generate large-scale

cluster entangled states. Fifteen quadripartite entangled cluster states were generated experimentally from a single optical parametric oscillator (OPO) in 2011 [10]. Sixty-mode cluster states in the quantum optical frequency comb were also demonstrated by experiment in 2014 [11]. Multimode entanglement frequency combs were obtained in a below-threshold synchronously pumped OPO in 2013 [12]. And the ultra-large-scale CV cluster entangled states in the time domain were generated sequentially in the same year [13]. Beyond that, we also proposed a scheme to generate a multiplexed entanglement frequency comb in a nondegenerate optical parametric amplifier [14] and got the low-frequency signal beyond shot-noise level from the optical frequency comb [15]. The optical spatial mode comb is another promising way to generate large-scale cluster entangled states in the spatial domain. The multispatial mode amplifier configuration was put forward in 2014, which can yield a dual-rail CV cluster state over the optical spatial mode comb in theory [16].

Based on the above research, we design a scheme to generate the spatial cluster entangled states of Laguerre–Gaussian mode utilizing two pump modes ( $lg_l^p$ , index  $l = \pm 1$  is referred to as the azimuthal mode index) with the same frequency ( $2\omega_0$ ) in a large-Fresnel-number (or self-imaging) degenerate optical parametric oscillator (DOPO) operating below threshold with type I phase matching. The large-Fresnel-number DOPO

cavity is constructed by spherical mirrors. And the self-imaging OPO cavity is composed of a plane mirror, a lens, and a spherical mirror. These two kinds of cavities can allow simultaneous and sustainable nonlinear interaction and resonance of several transverse modes [17,18].

In this paper, arrangements of details are outlined as follows: In Section 2, our theoretical model for CV spatial cluster entangled states is introduced concisely and the evolution equations of the spatial modes and quadrature fluctuation are deduced. Then we employ the boundary conditions of optical cavities to calculate the amplitude and phase quadratures of the spatial modes. In Section 3, the entanglement criterion proposed by van Loock and Furusawa for the inseparability of optical fields [19] is used to estimate whether there is entanglement among CV spatial cluster states of Laguerre–Gaussian modes. Finally, a brief summary is presented in Section 4.

## 2. THEORETICAL MODEL AND EQUATIONS DERIVATION

### A. Theoretical Model

The spatial cluster entangled states of Laguerre–Gaussian modes are generated in a large-Fresnel-number (or self-imaging) DOPO operating below threshold ( $\sigma < 1$ ), which is pumped by two spatial Laguerre–Gaussian modes ( $lg_l^p$ ) with the same frequency ( $2\omega_0$ ). There is a type I phase-matching nonlinear crystal  $\chi^{(2)}$  within the cavity. This kind of cavity can guarantee simultaneous and sustainable nonlinear interaction and resonance of all the pump and down-converted modes. A phase compensation piece or the crystal with special structure can be used to compensate the phase for different modes. Two pump fields of energy  $\hbar\omega_p$  can convert to two fields, signal and idler, of energy  $\hbar\omega_s$  and  $\hbar\omega_i$ , respectively. The nonlinear interaction must satisfy energy ( $\hbar\omega_p = \hbar\omega_s + \hbar\omega_i$ ,  $\omega_p = 2\omega_0$ ,  $\omega_s = \omega_i = \omega_0$ ), phase-matching ( $\hbar \rightarrow k_p = \hbar \rightarrow k_s + \hbar \rightarrow k_i$ ), and orbit angular momentum ( $l_p \hbar = l_s \hbar + l_i \hbar$ ) conservation [20]. The setup is described in Fig. 1.

The structure diagram of the down-converted Laguerre–Gaussian modes with degeneration frequency  $\omega_0$  is depicted in Fig. 2(a). All Einstein–Podolski–Rosen (EPR) pairs concatenate into the spatial Laguerre–Gaussian modes  $lg_{l,i}$  sequence ( $\dots lg_{-4}, lg_3, lg_{-2}, lg_1, lg_0, lg_{-1}, lg_2, lg_{-3}, lg_4 \dots$ ) [Fig. 2(a)].

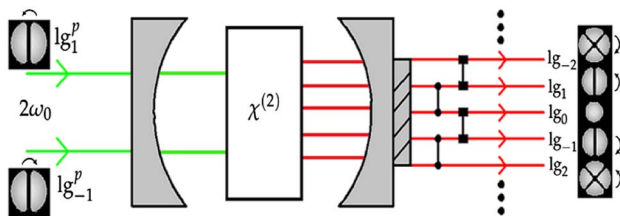


**Fig. 1.** Schematic: the two green lines represent the pump modes ( $lg_1^p, lg_{-1}^p$ ) with frequency ( $2\omega_0$ ), which can generate spatial Laguerre–Gaussian modes ( $lg_{l,i}$ , index  $l_{s,i} = \pm 1, \pm 2, \pm 3 \dots$  is also the azimuthal mode index) with frequency ( $\omega_0$ ) through parametric down-conversion. The black lines connecting solid circles and squares, respectively, represent the spatial modes generated by the pump fields  $lg_1^p$  and  $lg_{-1}^p$ . In a transverse plane, phase smoothly advances with angle  $\varphi$  along the direction of curved arrows, clockwise for  $l < 0$  and counterclockwise for  $l > 0$  in a transverse plane.

These EPR pairs of the spatial mode comb are connected by curved arrows, which compose a closed CV spatial cluster state. The quantum graph states of the spatial mode comb can be expressed as a dual-rail CV spatial cluster state in Fig. 2(b).

### B. Hamiltonian and Langevin Equations

The interaction Hamiltonian is

$$\hat{H} = i\hbar\chi^{(2)} \left[ \sum_{s=0}^{N/2} \hat{b}_{p_1} \hat{a}_s^\dagger \hat{a}_s^\dagger + \sum_{s=0}^{N/2} \hat{b}_{p_2} \hat{a}_s^\dagger \hat{a}_s^\dagger \right] + \text{H.C.},$$

with  $\chi^{(2)}$  representing the effective nonlinear coupling parameter;  $\hat{b}_{p_i}$  denoting the annihilation operators for the intra-cavity pump modes with the frequency  $2\omega_0$ ; and  $\hat{a}_s^\dagger$  and  $\hat{a}_s^\dagger$  being the creation operators of signal and idler modes with the frequency  $\omega_0$ .

For the periodicity of the structure diagram and dual-rail cluster states, we consider only two pump modes and seven down-converted modes for simplicity. The Langevin equations describing the evolution of the quadrature fluctuations inside the DOPO are given by

$$\begin{aligned} \tau \dot{\hat{b}}_1(t) &= -\gamma_p \hat{b}_1(t) + \epsilon_1 - \chi_1 \hat{a}_0(t) \hat{a}_1(t) - \chi_2 \hat{a}_{-1}(t) \hat{a}_2(t) \\ &\quad - \chi_3 \hat{a}_{-2}(t) \hat{a}_3(t) + \sqrt{2\gamma_{p_b}} \hat{b}_1^{\text{in}}(t) + \sqrt{2\gamma_{p_c}} \hat{c}_{b_1}(t), \\ \tau \dot{\hat{b}}_{-1}(t) &= -\gamma_p \hat{b}_{-1}(t) + \epsilon_{-1} - \chi_1 \hat{a}_0(t) \hat{a}_{-1}(t) - \chi_2 \hat{a}_1(t) \hat{a}_{-2}(t) \\ &\quad - \chi_3 \hat{a}_2(t) \hat{a}_{-3}(t) + \sqrt{2\gamma_{p_b}} \hat{b}_{-1}^{\text{in}}(t) + \sqrt{2\gamma_{p_c}} \hat{c}_{b_{-1}}(t), \\ \tau \dot{\hat{a}}_0(t) &= -\gamma_0 \hat{a}_0(t) + \chi_1 \hat{b}_1(t) \hat{a}_1^\dagger(t) + \chi_1 \hat{b}_{-1}(t) \hat{a}_{-1}^\dagger(t) \\ &\quad + \sqrt{2\gamma_{b_0}} \hat{a}_0^{\text{in}}(t) + \sqrt{2\gamma_{c_0}} \hat{c}_0(t), \\ \tau \dot{\hat{a}}_1(t) &= -\gamma_1 \hat{a}_1(t) + \chi_1 \hat{b}_1(t) \hat{a}_0^\dagger(t) + \chi_2 \hat{b}_{-1}(t) \hat{a}_{-2}^\dagger(t) \\ &\quad + \sqrt{2\gamma_{b_1}} \hat{a}_1^{\text{in}}(t) + \sqrt{2\gamma_{c_1}} \hat{c}_1(t), \\ \tau \dot{\hat{a}}_{-1}(t) &= -\gamma_{-1} \hat{a}_{-1}(t) + \chi_1 \hat{b}_{-1}(t) \hat{a}_0^\dagger(t) + \chi_2 \hat{b}_1(t) \hat{a}_2^\dagger(t) \\ &\quad + \sqrt{2\gamma_{b_{-1}}} \hat{a}_{-1}^{\text{in}}(t) + \sqrt{2\gamma_{c_{-1}}} \hat{c}_{-1}(t), \\ \tau \dot{\hat{a}}_2(t) &= -\gamma_2 \hat{a}_2(t) + \chi_2 \hat{b}_1(t) \hat{a}_1^\dagger(t) + \chi_3 \hat{b}_{-1}(t) \hat{a}_{-3}^\dagger(t) \\ &\quad + \sqrt{2\gamma_{b_2}} \hat{a}_2^{\text{in}}(t) + \sqrt{2\gamma_{c_2}} \hat{c}_2(t), \\ \tau \dot{\hat{a}}_{-2}(t) &= -\gamma_{-2} \hat{a}_{-2}(t) + \chi_2 \hat{b}_{-1}(t) \hat{a}_1^\dagger(t) + \chi_3 \hat{b}_1(t) \hat{a}_3^\dagger(t) \\ &\quad + \sqrt{2\gamma_{b_{-2}}} \hat{a}_{-2}^{\text{in}}(t) + \sqrt{2\gamma_{c_{-2}}} \hat{c}_{-2}(t), \\ \tau \dot{\hat{a}}_3(t) &= -\gamma_3 \hat{a}_3(t) + \chi_3 \hat{b}_1(t) \hat{a}_2^\dagger(t) + \sqrt{2\gamma_{b_3}} \hat{a}_3^{\text{in}}(t) \\ &\quad + \sqrt{2\gamma_{c_3}} \hat{c}_3(t), \\ \tau \dot{\hat{a}}_{-3}(t) &= -\gamma_{-3} \hat{a}_{-3}(t) + \chi_3 \hat{b}_{-1}(t) \hat{a}_2^\dagger(t) + \sqrt{2\gamma_{b_{-3}}} \hat{a}_{-3}^{\text{in}}(t) \\ &\quad + \sqrt{2\gamma_{c_{-3}}} \hat{c}_{-3}(t), \end{aligned} \quad (1)$$

where  $\tau$  is the round-trip time of the optical field inside the DOPO;  $\chi_1, \chi_2, \chi_3$  are the effective nonlinear coupling parameters; and  $\hat{b}_i$  and  $\hat{a}_i$  are the amplitude operators of the pump modes and the down-converted modes inside the cavity, respectively.  $\epsilon_1$  and  $\epsilon_{-1}$  are the pump fields that enter the cavity, which will be described classically.  $\hat{b}_i^{\text{in}}$  and  $\hat{a}_i^{\text{in}}$  denote the input amplitude operators of the pump modes and the down-converted modes.

In order to simplify the calculation, we suppose the two pump fields  $\epsilon_1$  and  $\epsilon_{-1}$  are identical. The losses of the pump

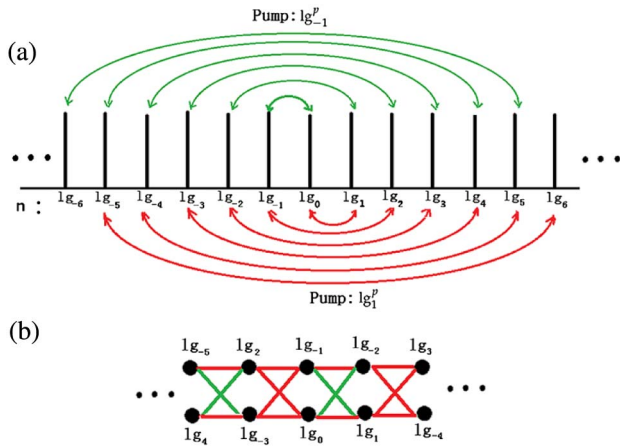


**Fig. 2.** (a) Structure diagram: the EPR pairs generated in the DOPO (at the same frequency  $n$  the mode is denoted by the black line). The green curved arrows (top) connecting EPR pairs are generated by pump  $1g_{-1}^p$ , and the red curved arrows (bottom) connecting EPR pairs are generated by pump  $1g_1^p$ . (b) Quantum graph states: the spatial modes, which are connected sequentially, can yield the dual-rail cluster states.

modes are defined as  $\gamma_p = \gamma_{p_b} + \gamma_{p_c}$ , where  $\gamma_{p_b}, \gamma_{p_c}$  correspond to the losses of output and intra-cavity losses for the pump modes. The output coupling losses and the intra-cavity losses are the same for the down-converted modes,  $\gamma_{b_0} = \gamma_{b_{\pm 1}} = \gamma_{b_{\pm 2}} = \gamma_{b_{\pm 3}} = \gamma_b$ ,  $\gamma_{c_0} = \gamma_{c_{\pm 1}} = \gamma_{c_{\pm 2}} = \gamma_{c_{\pm 3}} = \gamma_c$ . The total loss is  $\gamma = \gamma_b + \gamma_c$ ; therefore,  $\gamma_0 = \gamma_{\pm 1} = \gamma_{\pm 2} = \gamma_{\pm 3} = \gamma$ .

The nonlinear coupling parameter  $\chi^{(2)}$  is proportional to the overlap integral  $\Gamma_{p,i,s}$  between the down-converted modes and the pump modes in the transverse plane, that is,  $\chi_j = \Gamma_{p,i,s} \chi^{(2)}$ . The overlap integral is defined as [21]  $\Gamma_{p,s,i} = \int_{-\infty}^{\infty} u_p(r) u_s(r) u_i(r) dr$ . Here the expression of the Laguerre-Gaussian modes is given by [22]

$$u_{p,l}(r) = \sqrt{\frac{2p!}{\pi(p+|l|)!} \frac{1}{\omega(z)}} \left[ \frac{\sqrt{2}r}{\omega(z)} \right]^{|l|} L_p^{|l|} \left[ \frac{2r^2}{\omega(z)^2} \right] \exp[-il\phi] \\ \times \exp \left[ \frac{-r^2}{\omega(z)^2} - \frac{ikr^2}{2R(z)} \right] \exp \left[ -i(2p+|l|+1) \arctan \left( \frac{z}{z_R} \right) \right],$$

where  $\omega(z)$  is the size of the waist,  $L_p^{|l|}(x)$  is the generalized Laguerre polynomial,  $\arctan(z/z_R)$  is the Gouy phase (taking no account of it), and  $e^{-il\phi}$  represents the phase variation in a helical structure of the wavefront.

The overlap coefficients are given by Table 1 (we hypothesize that the phase matching is perfect and the parametric down-conversion (PDC) process meet the orbit angular momentum conservation). We consider only five pairs of down-converted modes from two pumps, respectively, because the overlap integrals of higher-order pairs are too small; thus 11-mode spatial cluster entangled states can be realized. Furthermore, in order

to have large parametric interaction and larger-scale entanglement, many details should be considered, such as perfect mode matching, alignment of interactional modes, and the structure of the special pump transverse mode. From Table 1, we can get the nonlinear coupling parameters:  $\chi_1 = \chi^{(2)}$ ,  $\chi_2 = 0.530\chi^{(2)}$ ,  $\chi_3 = 0.271\chi^{(2)}$ .

### C. Steady-State Solutions and Quadrature Fluctuations

The steady-state equation of Eq. (1) is then obtained to be

$$\begin{aligned} -\gamma_p \beta_1 + \epsilon - \chi_1 \alpha_0 \alpha_1 - \chi_2 \alpha_{-1} \alpha_2 - \chi_3 \alpha_{-2} \alpha_3 &= 0, \\ -\gamma_p \beta_{-1} + \epsilon - \chi_1 \alpha_0 \alpha_{-1} - \chi_2 \alpha_1 \alpha_{-2} - \chi_3 \alpha_2 \alpha_{-3} &= 0, \\ -\gamma \alpha_0 + \chi_1 \beta_1 \alpha_1^* + \chi_1 \beta_{-1} \alpha_{-1}^* &= 0, \\ -\gamma \alpha_1 + \chi_1 \beta_1 \alpha_0^* + \chi_2 \beta_{-1} \alpha_{-2}^* &= 0, \\ -\gamma \alpha_{-1} + \chi_1 \beta_{-1} \alpha_0^* + \chi_2 \beta_1 \alpha_2^* &= 0, \\ -\gamma \alpha_2 + \chi_2 \beta_1 \alpha_{-1}^* + \chi_3 \beta_{-1} \alpha_{-3}^* &= 0, \\ -\gamma \alpha_{-2} + \chi_2 \beta_{-1} \alpha_1^* + \chi_3 \beta_1 \alpha_3^* &= 0, \\ -\gamma \alpha_3 + \chi_3 \beta_1 \alpha_{-2}^* &= 0, \\ -\gamma \alpha_{-3} + \chi_3 \beta_{-1} \alpha_2^* &= 0, \end{aligned} \quad (2)$$

$$X \begin{pmatrix} \delta \hat{X}_{b_1}(\omega) \\ \delta \hat{X}_{b_{-1}}(\omega) \\ \delta \hat{X}_0(\omega) \\ \delta \hat{X}_1(\omega) \\ \delta \hat{X}_{-1}(\omega) \\ \delta \hat{X}_2(\omega) \\ \delta \hat{X}_{-2}(\omega) \\ \delta \hat{X}_3(\omega) \\ \delta \hat{X}_{-3}(\omega) \end{pmatrix} = X_1 \begin{pmatrix} \delta \hat{X}_{b_1}^{\text{in}}(\omega) \\ \delta \hat{X}_{b_{-1}}^{\text{in}}(\omega) \\ \delta \hat{X}_0^{\text{in}}(\omega) \\ \delta \hat{X}_1^{\text{in}}(\omega) \\ \delta \hat{X}_{-1}^{\text{in}}(\omega) \\ \delta \hat{X}_2^{\text{in}}(\omega) \\ \delta \hat{X}_{-2}^{\text{in}}(\omega) \\ \delta \hat{X}_3^{\text{in}}(\omega) \\ \delta \hat{X}_{-3}^{\text{in}}(\omega) \end{pmatrix} + X_2 \begin{pmatrix} \delta \hat{X}_{c_{b_1}}(\omega) \\ \delta \hat{X}_{c_{b_{-1}}}(\omega) \\ \delta \hat{X}_{c_0}(\omega) \\ \delta \hat{X}_{c_1}(\omega) \\ \delta \hat{X}_{c_{-1}}(\omega) \\ \delta \hat{X}_{c_2}(\omega) \\ \delta \hat{X}_{c_{-2}}(\omega) \\ \delta \hat{X}_{c_3}(\omega) \\ \delta \hat{X}_{c_{-3}}(\omega) \end{pmatrix}. \quad (3)$$

Here,  $\beta_{\pm 1}, \alpha_0, \alpha_{\pm 1}, \alpha_{\pm 2}, \alpha_{\pm 3}$  are the steady-state amplitudes of the modes  $b_{\pm 1}, a_0, a_{\pm 1}, a_{\pm 2}, a_{\pm 3}$ . The oscillation threshold  $\epsilon_{\text{th}}$  and the pump parameter  $\sigma$  are expressed by  $\epsilon_{\text{th}} = \sqrt{1 - 1/\sqrt{2}\gamma_p/\chi_1}$ ,  $\sigma = \epsilon/\epsilon_{\text{th}}$ . The steady-state solution of Eq. (2) below threshold ( $\sigma < 1$ ) is given by  $\beta_{\pm 1} = \epsilon/\gamma$ ,  $\alpha_0 = \alpha_{\pm 1} = \alpha_{\pm 2} = \alpha_{\pm 3} = 0$ . Through linearization we can set  $b_i = \beta_i + \delta b_i$ ,  $a_i = \alpha_i + \delta a_i$ ,  $a_i^{\text{in}} = \delta a_i^{\text{in}}$ . Substituting the quantum fluctuations into Eq. (1), and taking the Fourier transformation, we can obtain the fluctuation dynamics equations. Applying the definition of the amplitude and phase quadratures— $\hat{X} = \hat{a} + \hat{a}^\dagger$ ,  $\hat{Y} = (\hat{a} - \hat{a}^\dagger)/i$ —the amplitude quadratures of two pump modes and seven down-converted modes can be expressed in Eq. (3). In a similar way, the matrix form of the quadrature phase can be obtained. The coefficients of the matrix form are given by Eq. (4).

Using the boundary conditions [23]  $\delta \hat{X}_i^{\text{out}} = \sqrt{2\gamma_{b_i}} \delta \hat{X}_i - \delta \hat{X}_i^{\text{in}}$ ,  $\delta \hat{Y}_i^{\text{out}} = \sqrt{2\gamma_{b_i}} \delta \hat{Y}_i - \delta \hat{Y}_i^{\text{in}}$ , ( $i = 0, \pm 1, \pm 2, \pm 3$ ), we

**Table 1.** Overlap Integrals and Normalizations of the Down-converted Modes and Pump Modes

$p_1 = p_{-1}$	$\Gamma_{1,1,0} = \Gamma_{-1,-1,0}$	$\Gamma_{1,2,-1} = \Gamma_{-1,-2,1}$	$\Gamma_{1,3,-2} = \Gamma_{-1,-3,2}$	$\Gamma_{1,4,-3} = \Gamma_{-1,-4,3}$	$\Gamma_{1,5,-4} = \Gamma_{-1,-5,4}$
Overlap integral	0.849	0.450	0.230	0.116	0.058
Normalization	1	0.530	0.271	0.137	0.069

can obtain the amplitude and phase quadratures fluctuations of the output modes ( $\delta\hat{X}_0^{\text{out}}, \delta\hat{X}_{\pm 1}^{\text{out}}, \delta\hat{X}_{\pm 2}^{\text{out}}, \delta\hat{Y}_0^{\text{out}}, \delta\hat{Y}_{\pm 1}^{\text{out}}, \delta\hat{Y}_{\pm 2}^{\text{out}}$ ).

### 3. CHARACTERISTICS OF CV SPATIAL CLUSTER ENTANGLED STATES

The entanglements of CV spatial cluster states are indicated by the correlations of their amplitude and phase quadratures. The entanglement criterion proposed by van Loock and Furusawa for the inseparability of optical fields [19] can be used to testify the quantum entanglement of CV spatial cluster states:

$$\begin{aligned} S_{0,1} &= \Delta^2(\hat{X}_0^{\text{out}} - \hat{X}_1^{\text{out}} - g_1\hat{X}_{-1}^{\text{out}}) \\ &\quad + \Delta^2(\hat{Y}_0^{\text{out}} + \hat{Y}_1^{\text{out}} + g_2\hat{Y}_{-2}^{\text{out}}) < 4, \\ S_{-1,0} &= \Delta^2(\hat{X}_{-1}^{\text{out}} - \hat{X}_0^{\text{out}} - g_3\hat{X}_2^{\text{out}}) \\ &\quad + \Delta^2(\hat{Y}_{-1}^{\text{out}} + \hat{Y}_0^{\text{out}} + g_4\hat{Y}_1^{\text{out}}) < 4, \\ S_{2,-1} &= \Delta^2(\hat{X}_2^{\text{out}} - \hat{X}_{-1}^{\text{out}} - g_5\hat{X}_{-3}^{\text{out}}) \\ &\quad + \Delta^2(\hat{Y}_2^{\text{out}} + \hat{Y}_{-1}^{\text{out}} + g_6\hat{Y}_0^{\text{out}}) < 4, \\ S_{1,-2} &= \Delta^2(\hat{X}_1^{\text{out}} - \hat{X}_{-2}^{\text{out}} - g_7\hat{X}_{-3}^{\text{out}}) \\ &\quad + \Delta^2(\hat{Y}_1^{\text{out}} + \hat{Y}_{-2}^{\text{out}} + g_8\hat{Y}_3^{\text{out}}) < 4, \end{aligned}$$

where  $S_{0,1}, S_{-1,0}, S_{2,-1}, S_{1,-2}$  represent the quantum correlation spectra,  $\hat{X}_j^{\text{out}}$  and  $\hat{Y}_j^{\text{out}}$  ( $j = 0, \pm 1, \pm 2, \pm 3$ ) are the amplitude and phase quadratures operators of the output fields. The optimum  $g$  factor  $g_k$  ( $k = 1, 2, 3, \dots, 8$ ) can be obtained to be  $g_1 = g_4 = g_5 = g_6 = 0.4, g_2 = g_3 = g_7 = g_8 = 0.2$ :

$$\begin{aligned} X &= \begin{pmatrix} i\omega\tau + \gamma_p & 0 & 0 & 0 & 0 & 0 & 0 & 0 & 0 \\ 0 & i\omega\tau + \gamma_p & 0 & 0 & 0 & 0 & 0 & 0 & 0 \\ 0 & 0 & i\omega\tau + \gamma & -\chi_1\beta_1 & -\chi_1\beta_{-1} & 0 & 0 & 0 & 0 \\ 0 & 0 & -\chi_1\beta_1 & i\omega\tau + \gamma & 0 & 0 & -\chi_2\beta_{-1} & 0 & 0 \\ 0 & 0 & -\chi_1\beta_{-1} & 0 & i\omega\tau + \gamma & -\chi_2\beta_1 & 0 & 0 & 0 \\ 0 & 0 & 0 & 0 & -\chi_2\beta_1 & i\omega\tau + \gamma & 0 & 0 & -\chi_3\beta_{-1} \\ 0 & 0 & 0 & -\chi_2\beta_{-1} & 0 & 0 & i\omega\tau + \gamma & -\chi_3\beta_1 & 0 \\ 0 & 0 & 0 & 0 & 0 & 0 & -\chi_3\beta_1 & i\omega\tau + \gamma & 0 \\ 0 & 0 & 0 & 0 & 0 & -\chi_3\beta_{-1} & 0 & 0 & i\omega\tau + \gamma \end{pmatrix}, \\ Y &= \begin{pmatrix} i\omega\tau + \gamma_p & 0 & 0 & 0 & 0 & 0 & 0 & 0 & 0 \\ 0 & i\omega\tau + \gamma_p & 0 & 0 & 0 & 0 & 0 & 0 & 0 \\ 0 & 0 & i\omega\tau + \gamma & \chi_1\beta_1 & \chi_1\beta_{-1} & 0 & 0 & 0 & 0 \\ 0 & 0 & \chi_1\beta_1 & i\omega\tau + \gamma & 0 & 0 & \chi_2\beta_{-1} & 0 & 0 \\ 0 & 0 & \chi_1\beta_{-1} & 0 & i\omega\tau + \gamma & \chi_2\beta_1 & 0 & 0 & 0 \\ 0 & 0 & 0 & 0 & \chi_2\beta_1 & i\omega\tau + \gamma & 0 & 0 & \chi_3\beta_{-1} \\ 0 & 0 & 0 & \chi_2\beta_{-1} & 0 & 0 & i\omega\tau + \gamma & \chi_3\beta_1 & 0 \\ 0 & 0 & 0 & 0 & 0 & 0 & \chi_3\beta_1 & i\omega\tau + \gamma & 0 \\ 0 & 0 & 0 & 0 & 0 & \chi_3\beta_{-1} & 0 & 0 & i\omega\tau + \gamma \end{pmatrix}, \end{aligned}$$

$$X_1 = Y_1 = \text{diag} \left[ \sqrt{2\gamma_b}, \sqrt{2\gamma_b}, \sqrt{2\gamma_b}, \sqrt{2\gamma_b}, \sqrt{2\gamma_b}, \sqrt{2\gamma_b}, \sqrt{2\gamma_b}, \sqrt{2\gamma_b}, \sqrt{2\gamma_b} \right],$$

$$X_2 = Y_2 = \text{diag} \left[ \sqrt{2\gamma_c}, \sqrt{2\gamma_c}, \sqrt{2\gamma_c}, \sqrt{2\gamma_c}, \sqrt{2\gamma_c}, \sqrt{2\gamma_c}, \sqrt{2\gamma_c}, \sqrt{2\gamma_c}, \sqrt{2\gamma_c} \right]. \quad (4)$$

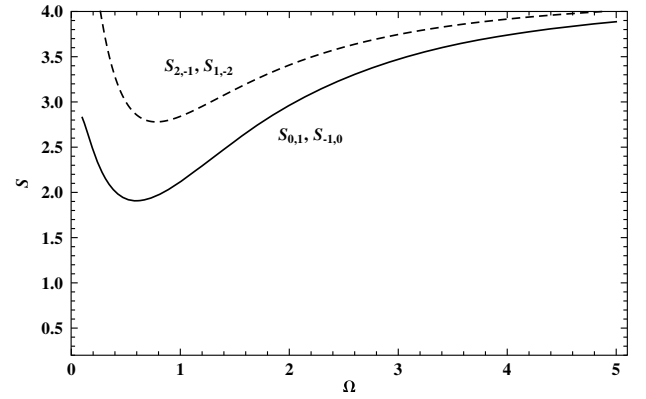


**Fig. 3.** Quantum correlation spectra  $S_{0,1}, S_{-1,0}, S_{2,-1}$ , and  $S_{1,-2}$  versus normalized analyzing frequency  $\Omega = \omega\tau/\gamma$  with  $\gamma_p = 0.03, \gamma_{p_0} = 0.028, \gamma_{p_c} = 0.002, \gamma = 0.02, \gamma_b = 0.018, \gamma_c = 0.002, \chi_1 = \chi^{(2)}, \chi_2 = 0.530\chi^{(2)}, \chi_3 = 0.271\chi^{(2)}$ , and  $\sigma = 0.9$ .

Figure 3 clearly shows that the quantum correlation spectra of  $S_{0,1}, S_{-1,0}, S_{2,-1}$ , and  $S_{1,-2}$  versus normalized analyzing frequency  $\Omega = \omega\tau/\gamma$ . They all satisfy the criterion and their entanglement properties are similar. First, the entanglement degree grows with the normalized analyzing frequency and exhibits maximum entanglement at  $\Omega = 0.65$ . Then, the entanglement decreases gradually and disappears roughly at  $\Omega = 5$ . It is evident that the correlations are existent in a wide range of

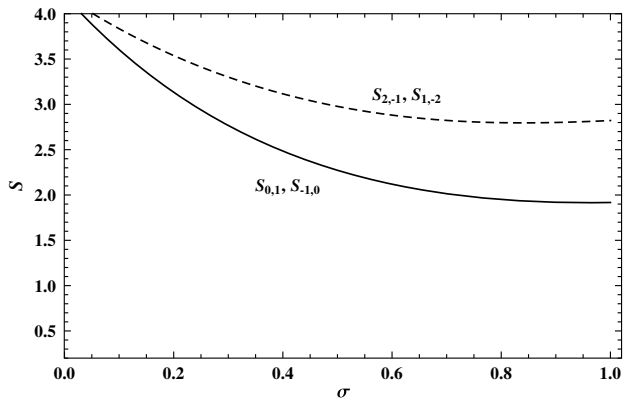


**Fig. 4.** Quantum correlation spectra  $S_{0,1}$ ,  $S_{-1,0}$ ,  $S_{2,-1}$ , and  $S_{1,-2}$  versus pump parameter  $\sigma = \epsilon/\epsilon_{\text{th}}$  with  $\gamma_p = 0.03$ ,  $\gamma_{pb} = 0.028$ ,  $\gamma_{pc} = 0.002$ ,  $\gamma = 0.02$ ,  $\gamma_b = 0.018$ ,  $\gamma_c = 0.002$ ,  $\chi_1 = \chi^{(2)}$ ,  $\chi_2 = 0.530\chi^{(2)}$ ,  $\chi_3 = 0.271\chi^{(2)}$ , and  $\Omega = 0.65$ .

normalized analyzing frequency when we select the optimized pump parameter  $\sigma = 0.9$ .

Figure 4 shows the quantum correlation spectra of  $S_{0,1}$ ,  $S_{-1,0}$ ,  $S_{2,-1}$ , and  $S_{1,-2}$  versus pump parameter  $\sigma = \epsilon/\epsilon_{\text{th}}$  (normalized to the pump threshold). The largest entanglement degree can be obtained near the threshold of the DOPO. The CV spatial cluster entangled state generated from the DOPO operating below the threshold ( $\sigma < 1$ ) can be realized within a wide pump parameter range.

As clearly shown in Figs. 3 and 4, the correlation spectra satisfy  $S_{0,1} = S_{-1,0}$ , because the spatial mode EPR pairs  $lg_0 \sim lg_1$  and  $lg_{-1} \sim lg_0$  corresponding to the same nonlinear coupling parameter  $\chi_1$ ; similarly,  $S_{2,-1} = S_{1,-2}$ . In addition, for the nonlinear coupling parameter  $\chi_1 > \chi_2$ , the correlation spectra of  $S_{0,1}$ ,  $S_{-1,0}$  are always lower than the correlation spectra of  $S_{2,-1}$ ,  $S_{1,-2}$ . We testify the deterministic entanglement among five spatial Laguerre–Gaussian modes by considering all related noise of seven modes. Finally, we believe that at least 11-partite spatial cluster entangled states of Laguerre–Gaussian modes can be produced when considering the overlap integral of the parametric modes and the periodicity of quantum graph states.

For this scheme, we can use a two-tone balanced homodyne detection with the spatially tailored local oscillator modes to measure the amplitude and phase quadratures in real experiment. The results of the addition or subtraction for the amplitude and phase quadratures are fed into a spectrum analyzer, which is set to display the noise power. In this way, the level of entanglement can be created by reporting the amount of squeezing.

#### 4. CONCLUSION

In summary, we theoretically propose a scheme to generate CV spatial cluster entangled states of Laguerre–Gaussian modes from the DOPO and use the criterion proposed by van Loock and Furusawa for the inseparability to estimate entanglement among CV spatial cluster states. Eleven-partite spatial cluster entangled states of Laguerre–Gaussian modes can be produced with strong pump power and big  $\chi^{(2)}$ . Based on this scheme, for higher-order PDC, the creation conditions, quantum dynamical equation, and the boundary conditions,

etc., are the same while the nonlinear coupling parameters are different. Therefore, if we have stronger power and optimal mode for pump, bigger  $\chi^{(2)}$  and higher overlap integral, a large-scale cluster entangled state (more than 11-partite) will be achieved. This scheme provides theoretical basis and experimental guidance for further realization of large-scale spatial entanglement states, which is a versatile resource for facilitating fundamental studies of measurement-based quantum computation, quantum information processing, and quantum image.

**Funding.** National Natural Science Foundation of China (NSFC) (11504218, 61108003, 91536222, 61405108); Natural Science Foundation of Shanxi Province, China (2013021005-2); National Key Research and Development Plan (2016YFA0301404).

#### REFERENCES

1. T. J. Johnson, S. D. Bartlett, and B. C. Sanders, “Continuous-variable quantum teleportation of entanglement,” *Phys. Rev. A* **66**, 042326 (2002).
2. S. L. Braunstein and H. J. Kimble, “Dense coding for continuous variables,” *Phys. Rev. A* **61**, 042302 (2000).
3. L. S. Madsen, V. C. Usenko, M. Lassen, R. Filip, and U. L. Andersen, “Continuous variable quantum key distribution with modulated entangled states,” *Nat. Commun.* **3**, 1083 (2012).
4. G. Adesso, A. Serafini, and F. Illuminati, “Multipartite entanglement in three-mode Gaussian states of continuous-variable systems: quantification, sharing structure, and decoherence,” *Phys. Rev. A* **73**, 032345 (2006).
5. J. Zhang and S. L. Braunstein, “Continuous-variable Gaussian analog of cluster states,” *Phys. Rev. A* **73**, 032318 (2006).
6. P. van Loock, C. Weedbrook, and M. Gu, “Building Gaussian cluster states by linear optics,” *Phys. Rev. A* **76**, 032321 (2007).
7. P. van Loock and S. L. Braunstein, “Multipartite entanglement for continuous variables: a quantum teleportation network,” *Phys. Rev. Lett.* **84**, 3482–3485 (2000).
8. Y. H. Ma, G. H. Yang, Q. X. Mu, and L. Zhou, “Greenberger-Horne-Zeilinger state generation among remote nodes,” *J. Opt. Soc. Am. B* **26**, 713–717 (2009).
9. P. Dong, Z. Y. Xue, M. Yang, and Z. L. Cao, “Generation of cluster states,” *Phys. Rev. A* **73**, 033818 (2006).
10. M. Pysker, Y. Miwa, R. Shahrokshahi, R. Bloomer, and O. Pfister, “Parallel generation of quadripartite cluster entanglement in the optical frequency comb,” *Phys. Rev. Lett.* **107**, 030505 (2011).
11. M. Chen, N. C. Menicucci, and O. Pfister, “Experimental realization of multipartite entanglement of 60 modes of a quantum optical frequency comb,” *Phys. Rev. Lett.* **112**, 120505 (2014).
12. J. Roslund, R. Medeiros de Araujo, S. Jiang, C. Fabre, and N. Treas, “Wavelength-multiplexed quantum networks with ultrafast frequency combs,” *Nat. Photonics* **8**, 109–112 (2014).
13. S. Yokoyama, R. Ukai, S. C. Armstrong, C. Sornphiphatphong, T. Kaji, S. Suzuki, J.-I. Yoshikawa, H. Yonezawa, N. C. Menicucci, and A. Furusawa, “Ultra-large-scale continuous-variable cluster states multiplexed in the time domain,” *Nat. Photonics* **7**, 982–986 (2013).
14. R. G. Yang, J. Zhang, S. Q. Zhai, K. Liu, J. X. Zhang, and J. R. Gao, “Generating multiplexed entanglement frequency comb in a nondegenerate optical parametric amplifier,” *J. Opt. Soc. Am. B* **30**, 314–318 (2013).
15. R. G. Yang, J. Zhang, Z. H. Zhai, S. Q. Zhai, K. Liu, and J. R. Gao, “Scheme for efficient extraction of low-frequency signal beyond the quantum limit by frequency-shift detection,” *Opt. Express* **23**, 21323–21333 (2015).
16. R. Pooser and J. T. Jing, “Continuous-variable cluster-state generation over the optical spatial mode comb,” *Phys. Rev. A* **90**, 043841 (2014).
17. C. N. Benlloch, G. J. de Valcarcel, and E. Roldan, “Generating highly squeezed hybrid Laguerre-Gauss modes in large-Fresnel-number

- degenerate optical parametric oscillators," *Phys. Rev. A* **79**, 043820 (2009).
18. B. Chalopin, F. Scazza, C. Fabre, and N. Treps, "Direct generation of a multi-transverse mode non-classical state of light," *Opt. Express* **19**, 4405–4410 (2011).
  19. P. van Loock and A. Furusawa, "Detecting genuine multipartite continuous-variable entanglement," *Phys. Rev. A* **67**, 052315 (2003).
  20. M. Lassen, G. Leuchs, and U. L. Andersen, "Continuous variable entanglement and squeezing of orbital angular momentum states," *Phys. Rev. Lett.* **102**, 163602 (2009).
  21. M. Lassen, V. Delaubert, C. C. Harb, P. K. Lam, N. Treps, and H.-A. Bachor, "Generation of squeezing in higher order Hermite-Gaussian modes with an optical parametric amplifier," *J. Eur. Opt. Soc.* **1**, 06003 (2006).
  22. A. Vaziri, G. Weihs, and A. Zeilinger, "Superpositions of the orbital angular momentum for applications in quantum experiments," *J. Opt. B* **4**, S47–S51 (2002).
  23. M. J. Collett and C. W. Gardiner, "Squeezing of intracavity and traveling-wave light fields produced in parametric amplification," *Phys. Rev. A* **30**, 1386–1391 (1984).